ROYAL SOCIETY
OF CHEMISTRY

Check for updates

Highly efficient Zn$_{1-x}$Cd$_x$S catalysts with sphalerite structures synthesized *via* a novel green method for hydrogen production by water splitting†

M. González-Rodríguez, [ID] ab S. Díaz-Coello, [ID] ab S. Díaz-González, [ID] a
V. D. Rodríguez, [ID] c M. Žitňan, [ID] d G. Galleani, [ID] d J. J. Velázquez, [ID] d E. Pastor [ID] ab
and P. Núñez [ID] *ab

The present study focuses on the development of a photochemical reactor coupled with a mass spectrometer for the *in situ* detection of the H$_2$ generation rate of the photochemical water splitting process. To do so, sphalerite-type Zn$_{1-x}$Cd$_x$S catalysts were synthesized, characterized, and tested as a proof-of-concept for the development of the equipment with applied materials. The sulphides were obtained by means of a green synthetic method, which avoids the use of toxic non-aqueous solvents and the application of high temperatures. The prepared Zn/Cd sulphide catalysts were physicochemically characterized by XRD, TEM, diffuse reflectance spectroscopy and electrochemical impedance spectroscopy. Afterwards, the catalytic performance of the materials towards hydrogen (photo) production was studied by means of the photoreactor coupled with the mass spectrometer. On the one hand, the results show the suitability of the photoreactor designed to measure the reaction rate under *in situ* conditions, exhibiting clear changes in the scan rate upon increasing the light energy (from visible to UV light). On the other hand, a high hydrogen production was achieved for Zn$_{0.7}$Cd$_{0.3}$S with a maximum value of 29.5 mmol g$_{cat}^{-1}$ after 100 minutes under visible light. This production is significantly higher than those previously reported in the literature for other standard materials, indicating the high potential of our materials for green hydrogen production.

1. Introduction

The end of the 20th century and the beginning of the new millennium has been marked by the environmental and fuel crisis,[1] among other political problems. Therefore, in recent decades, scientists and engineers have investigated new routes to achieve clean and sustainable energy that does not depend on fossil fuels.[2] In this regard, hydrogen has been proposed as a suitable alternative. However, it is hardly found in nature, and therefore, it is desirable to develop better and cheaper ways to produce it at high purity levels. Nowadays, hydrogen production is based on the exploitation of non-renewable sources, such as gas and coal (normally labelled as non-environmental or grey

hydrogen). The production of hydrogen through environmentally renewable sources (also known as green hydrogen) is still in its initial stages. Thus, the global production of green H$_2$ was lower than 2% of the total production in 2021.[3] For this reason, it is necessary to increase both research and investment in the next years. Several alternative methods have been proposed for producing green hydrogen, aiming to achieve higher production rates, lower costs, and the use of renewable sources to boost the procedure. In this sense, hydrogen photoproduction through water splitting has become an interesting option to fulfil these necessities.[4] Diverse sustainable strategies on the green hydrogen production have been proposed. Among them, photocatalysis is probably the cheapest and easiest method.[5,6]

In 1972, Honda and Fujishima[7,8] reported that water could be broken down into its elementary atoms (H$_2$ and O$_2$), by means of the water splitting technique onto a TiO$_2$ surface.[9] This technique consists of breaking the water molecules into molecular oxygen and hydrogen using UV and visible radiation.[10] However, the rapid recombination of the photoexcited electrons and holes hinder this process, leading to an inefficient exploitation of visible light, which is among the other limitations of TiO$_2$ in photocatalytic reactions.[11] The current trend is the use of co-catalysts to reduce the recombination of electrons and holes and the activation energy. Instead, significant

*a*Departamento de Química, U.D. Química Inorgánica, Universidad de La Laguna, Apto. 456, 38200 La Laguna, Tenerife, Spain. E-mail: pnunez@ull.es

*b*Instituto de Materiales y Nanotecnología, Universidad de La Laguna, Apto. 456, 38200 La Laguna, Tenerife, Spain

*c*Departamento de Física, Universidad de La Laguna, Apto. 456, 38200 La Laguna, Tenerife, Spain

*d*FunGlass, Alexander Dubcek University of Tencin, Studentska 2, 91150 Trencin, Slovakia

research efforts have been devoted to the search of semi-conductor materials for water splitting, such as metal-doped and undoped oxides,[12-14] (oxy)nitrides,[15,16] sulfides,[17] *etc.*, as well as free-metal carbon materials (g-C₃N₄).[18] The typical metals[5,19,20] used for doping are usually those with an electronic configuration of d⁰ and d¹⁰.

Both CdS and ZnS show wurtzite (ICSD: #154187) and sphalerite (ICSD: #81925) polymorphs. The latter is derived from cubic closest packing, while the first one comes from hexagonal closest packing. That means both crystal structures are quite close, and one can obtain wurtzite or sphalerite depending on the synthesis conditions. Most of the existing works on CdS for the sphalerite structure are heterojunctions of the sphalerite and wurtzite structure.[21-23] It has been reported[24-31] that the properties of CdS can be improved by forming nanocomposite structures with other functional nanomaterials, or by establishing heterojunctions between the different polymorphs.[32,33] In this sense, a good example is the zinc sulphide structures doped with cadmium, $Zn_{1-x}Cd_xS$, which presents higher activity due to the change in the positions of the valence and conduction bands.[34,35] However, few authors have studied this compound under UV light conditions,[36-38] and no previous studies have been found for the polymorph sphalerite under these conditions. This family of compounds is controversial because the maximum hydrogen production is not always obtained for the same composition.[39] To explain this, several DFT-based theoretical calculations of free energy have been reported for related reactions on ZnS and CdS surfaces.[40] Other studies suggest that the strength of this family of compounds is directly related to the position of the valence band, having enough redox power with an optimal band gap value to allow it to absorb a large amount of radiation from the visible spectrum onwards.[32,36] This is mainly because the addition of cadmium to the system reduces the band gap, but maintains the conduction band at values close to 3 eV, which is considered a suitable value for water splitting. It is well known that noble metals such as rhodium, palladium and platinum dramatically enhance the efficiency of hydrogen evolution for CdS. However, platinum loading on ZnS shows limited improvement. Moreover, the high cost of noble metals limits their large-scale application.[41,42] One significant challenge is to find a high-performance non-noble metal cocatalyst.[14,43-45] Transition metal co-catalysts, metal–organic frameworks, or carbon-based nanocomposites are some promising options.[46-48] For example, the addition of nickel or cobalt oxides significantly improves hydrogen production for CdZnS compounds.[49,50] The $Zn_{1-x}Cd_xS$ photocatalyst exhibited better stability in the presence of Na₂S and Na₂SO₃ as the sacrificial agent, whereas it exhibited relatively poor stability in the presence of ethanol.[51] When no sacrificial agents are present, the reactions that take place for CdS are as follows:[52,53]

$$h\nu \xrightarrow{CdS} h^+ + e^- \tag{1}$$

$$CdS + 2h^+ \rightarrow Cd^{2+} + S \tag{2}$$

$$2H_2O + 2e^- \rightarrow H_2 + 2OH^- \tag{3}$$
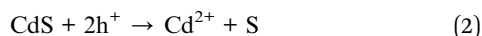
The sacrificial agent plays a fundamental role in preventing the corrosion that occurs on the catalyst. This problem was addressed by Ningzhong Bao *et al.*[54] The photogenerated electrons in eqn (1) are employed in eqn (3) to give rise to hydrogen production. At the same time, the generated holes (eqn (1)) react in two pathways: (a) sulphite ions (SO_3^{2-}) are oxidized to sulfate ions (SO_4^{2-}); and (b) sulfide ions (S^{2-}) are oxidized to disulfide ions (S_2^{2-}):

$$SO_3^{2-} + 2OH^- + 2h^+ \rightarrow SO_4^{2-} + H_2O \tag{4}$$

$$2S^{2-} + 2h^+ \rightarrow S_2^{2-} \tag{5}$$
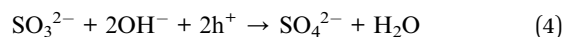
The S_2^{2-} ions present two problems: (a) they act as a light filter due to its yellowish coloration; and (b) they compete in the proton reduction reaction. However, with the presence of SO_3^{2-} ions in the medium, the following reaction takes place:

$$S_2^{2-} + SO_3^{2-} \rightarrow S_2O_3^{2-} + S^{2-} \tag{6}$$
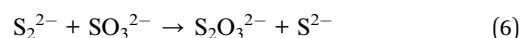
The presence of disulfide ions, S_2^{2-}, in solution stabilizes the catalyst and inhibits the appearance of surface defects. This phenomenon, together with the processes described in eqn (4) and (5), help to stabilize and reduce the photocorrosion produced in the catalyst.[54]

In this study, the $Zn_{1-x}Cd_xS$ solid solution has been prepared in a facile and environmentally friendly way, and was subsequently structurally and electrochemically characterized. We combined two approaches to address the stability: doping CdS with ZnS, and using a Na₂S/Na₂S₂O₃-based sacrificial agent by keeping the synthesis route simple and environmentally friendly. We then studied the hydrogen production by water splitting using the obtained catalysts.

2. Experimental

2.1 Reagents

The following reagents were purchased and used without further purification steps: Cd(CH₃COO)₂·2H₂O (Merck, 99.5%); Zn(CH₃COO)₂·2H₂O (Merck, 99%); Na₂S·xH₂O (Aldrich, >60%); Na₂SO₃ (VWR-Chemicals, 98.1%), CdCl₂ H₂O (Aldrich, 98%); ZnCl₂ (Merck, 98%); CS₂ (Merck, 99.5%); ethylenediamine (Merck, synthesis grade); ethanol (Scharlau, 70%); butanol (Panreac, 99.5%); Nafion® (5%, Sigma-Aldrich); argon (Air Products, 99.999%). TGA was carried out to determine the number of water molecules in the hydrate compound, Na₂S·xH₂O.

2.2 Preparation of $Zn_{1-x}Cd_xS$

2.2.1 $Zn_{1-x}Cd_xS$ with sphalerite structure. A typical synthesis was performed by dissolving 10 mmol of zinc/cadmium acetate in 50 mL of distilled water to prepare a 0.2 M solution in metal. Another solution of 25 mmol of Na₂S in 50 mL of distilled water was prepared (0.5 M in S^{2-}). The first solution was added dropwise very slowly over the latter and with stirring, which was maintained for 1 hour at room temperature. The resulting solid was separated by centrifugation at 4200 rpm

for 10 minutes, washed twice with cold deionized water and once with ethanol, with centrifugation each time. Subsequently, it was dried overnight in an oven at 60 °C. A very fine yellowish powder of $Zn_{1-x}Cd_xS$ was obtained, with $x = 0.0$; 0.2; 0.5; 0.7; 0.8; and 1.0.

2.2.2 ZnS/CdS with wurtzite structure. The synthesis was performed following a modification of the method described elsewhere.[55] In a typical synthesis, 4 mmol of zinc/cadmium chloride was dissolved in 5 mL of deionized water and 15 mL of butanol. Then, 30 mL of ethylenediamine was added drop-wise to this solution, followed by 0.5 g of CS_2. This mixture was heated by reflux for 1 hour. The resulting powder was obtained by centrifugation, washed twice with water and once with ethanol, and dried at 60 °C overnight.

2.3 Characterization

The XRD patterns were performed with an Empyrean PAN-alytical X-ray diffractometer using Cu K_α radiation ($\alpha = 1.54056$ Å) in a 2θ range from 10° to 80°. The phase identification was performed using the X'Pert HighScore Plus software with the PDF-4 database. For the transmission electron microscopy study (TEM 200 kV, Jeol JEM 2100), the sample was prepared by suspending 25 mg of catalyst in absolute ethanol in an ultrasonic bath for 20 minutes. Subsequently, a portion of the dispersion was taken, and a drop was deposited onto carbon-coated copper TEM grids. The diffuse reflectance spectra (DRS) were recorded using a UV-visible spectrophotometer from Agilent Technologies, model Cary 5000. $BaSO_4$ powder, used as the reference, was mixed in a mortar with the photocatalyst. The Fluorolog FL3-21 fluorescence spectrophotometer (Jobin Yvon HORIBA) was used to record steady-state luminescence spectra of the selected samples in the VIS region at room temperature in front face mode (back-scattering geometry) using an Xe lamp (450 W) as the excitation light source. A photomultiplier tube R928 detector was used to collect the signal.

Electrochemical impedance spectroscopy (EIS) was carried out with an Autolab potentiostat/galvanostat equipped with a frequency response analyser (Autolab-PGSTAT204-FRA32M) to achieve the flat-band potential (V_{FB}) and an estimation of the location of the conduction band. A glass three-electrode half-cell was used to perform the EIS experiments with 0.1 M Na_2SO_3 as the background electrolyte. The electrode setup consisted of a reversible hydrogen electrode (RHE) in the supporting electrolyte as the reference electrode and a glassy carbon (GC) rod as the auxiliary electrode. The potentials in this work are referred to the RHE. As the working electrode, several catalyst inks were produced and drop-casted onto the surface of a glassy carbon disk (geometric area = 0.0706 cm^2). The inks were achieved by sonication of 4 mg of photocatalyst in 15 µL of Nafion and 5 mL of ultrapure water, and then 10 µL of the ink was immobilized onto the GC disk under argon flux. After the immersion of the working electrode, the capacitance of the system was recorded at 1000, 1500 and 2000 Hz in a potential range between −0.7 and 0.0 V, applying potential steps of 50 mV. After the experiments, the validity of the Mott–Schottky

plots was assessed[56] and the value of the flat-bands was obtained.

Hydrogen photocatalytic production was studied by means of a configuration designed and built in our laboratory, as described previously.[14,42] Briefly, this system includes an elliptical-based cylindrical reflecting wall, which generates two focal points. Thus, the reactor is placed in one of the focal points of the ellipse and the radiation lamps in the other one. Using this configuration, a homogeneous reflection of the light is produced and concentrating at the reactor focus through the geometry of the ellipsis. The latter consists of a double-walled borosilicate flask that allows a flow of water in the inner wall for temperature control purposes during the experiment. UV mercury (Philips, HPA Synergy 300 W) and visible (Leuci Classic Halogen linear, 500 W) lamps were used as radiation sources. Hydrogen photochemical production was monitored continuously using an Omnistar mass spectrometer (Pfeiffer Vacuum) connected to the reactor outlet by a PTFE capillary. Additionally, a continuous nitrogen gas transport flow of 15 mL min^{-1} was passed through the reactor set by a mass flow controller. To quantify the amount of hydrogen produced, the H_2 channel signal provided by the mass spectrometer was previously calibrated with the carrier gas and different concentrations of pure hydrogen.

In all experiments, 0.200 g of $Zn_{1-x}Cd_xS$ powder was added to the reactor containing 200 mL of a solution with 0.35 M Na_2S and 0.25 M Na_2SO_3,[47,57,58] which will act as a sacrificial agent. The measurements were carried out under visible light for 100 minutes, and switched to UV light for another 100 minutes. The suspension was kept under continuous stirring and the reactor temperature was maintained at 20 °C, using a water flow into the reactor jacket from a thermostat bath (Selecta, model 382), throughout the whole measurement processes.

3. Results and discussion

3.1 X-ray patterns and morphological analysis

Fig. 1 shows the X-ray diffraction patterns of the synthesized CdS particles with both crystalline structures: wurtzite (Fig. 1A) and sphalerite (Fig. 1B). These patterns were compared with the references from the ICSD database: #81925 (sphalerite)[59] and #154187 (wurtzite).[60] The XRD patterns for the synthesized target materials ($Zn_{1-x}Cd_xS$, see Fig. 1C) present the characteristic Bragg peak features corresponding to metal sulphides with a sphalerite structure. For the pure sphalerite-type sulphide structures, the patterns reveal the $F\bar{4}3m$ space group (#216), presenting a cell parameter a of 5.80 Å for the CdS. The latter decreases to 5.36 Å for the ZnS, as it has been already reported for similar materials (5.77 Å and 5.33 Å, respectively). Upon increasing the amount of cadmium content in the $Zn_{1-x}Cd_xS$ sphalerite phase, the main Bragg peaks of the zinc sulphide remain. However, the peak positions are slightly shifted towards smaller angles. This reveals the complete formation of a solid solution of the two metal cations without the existence of any other secondary phases. Considering that both share a tetrahedral coordination, the downshifting of the mixed sulphide peaks in comparison with ZnS arises since the
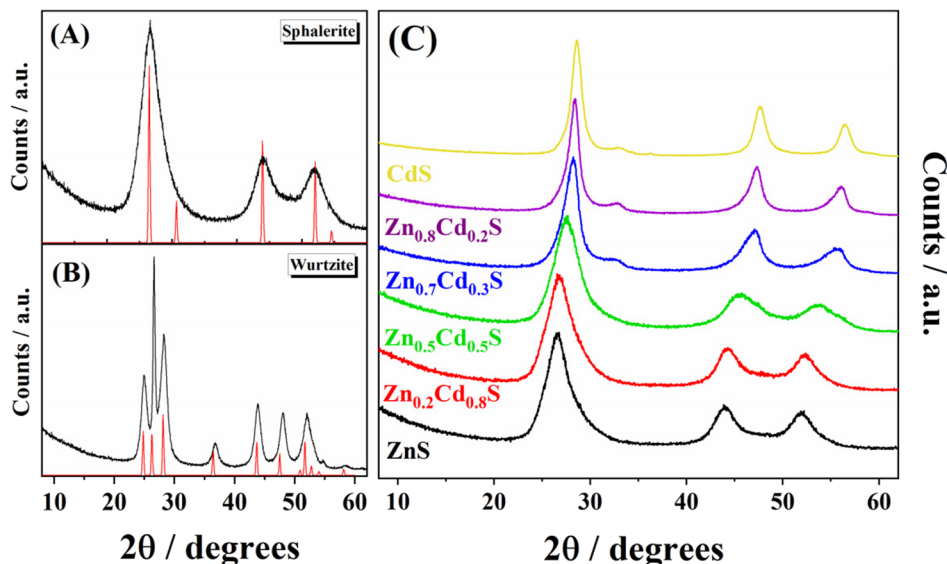
Fig. 1 X-ray diffraction patterns for (A) experimental (black) and reference (red) (ICSD #81925) CdS with sphalerite structure. (B) Experimental (black) and reference (red) CdS wurtzite structure (ICSD #154187) (C) X-ray diffraction patterns of the synthesized $Zn_{1-x}Cd_xS$, with x values ranging from 0 to 1.

radius of Zn^{2+} (0.74 Å) is smaller than the radius of Cd^{2+} (0.94 Å).[61,62] Additionally, all experimental patterns display very wide Bragg peaks, proving that sulphide crystallites were obtained at the nanometric scale.[57,58,63] The latter was corroborated by means of transmission electron microscopy, as shown in Fig. 2. As shown in Fig. 2A, the $Zn_{1-x}Cd_xS$ solid solution prepared in the present work does not exhibit the typical needle morphology of the metal sulphide with wurtzite structure.[64] Instead, small and rather spherical particles (8.5 nm) have been obtained. In addition, Fig. 2B reveals the atomic domains of the different nanoparticles along with the identification of the (111) crystalline planes, presenting an interplanar distance of 0.331 nm.

3.2 Determination of bandgaps

As the materials described above were designed for testing our home-made *in situ* mass spectrometer photocatalytic reactor, further insights about the semiconductor features of the materials are needed. Thus, the band gap energy, as well as the conduction and valence band positions, were estimated by both spectroscopic and electrochemical methods, respectively. Firstly, the band gap was estimated by means of UV-vis diffuse reflectance spectroscopy (see Fig. 3A) and the Tauc plots were subsequently obtained by applying the following equation:

$$C(h\nu - E_g) = (\alpha h\nu)^{1/n} \tag{7}$$

Where h is the Planck constant; ν is the frequency; E_g is the bandgap energy, C is a constant, n is 2 (as the materials present a direct allowed transition semiconductor behaviour), and α is the absorption coefficient of the semiconductor, calculated from the reflectance spectra by using the Kubelka–Munk model.[65–67] The results for the band gap energy determination are depicted in Fig. 3B. For the sake of clarity, only the ZnS, $Zn_{0.7}Cd_{0.3}S$ and CdS values are given. All values are presented in Fig. S1, ESI.† In this way, the value of the latter can be obtained from the extrapolation of the slope at the place where it cuts the abscissa axis. In the case of CdS and ZnS, the bandgaps are 2.55 eV and 3.60 eV, respectively. These values are close to the
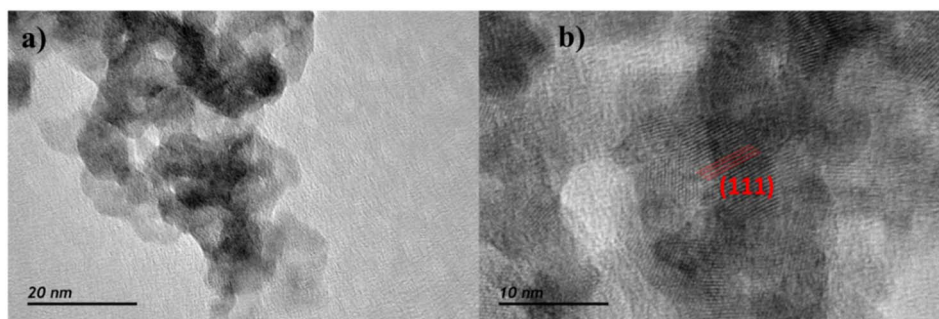

Fig. 2 (a) TEM image and (b) HRTEM image showing the domains within a particle corresponding to the (111) diffraction plane. Both images are of $Zn_{0.7}Cd_{0.3}S$.

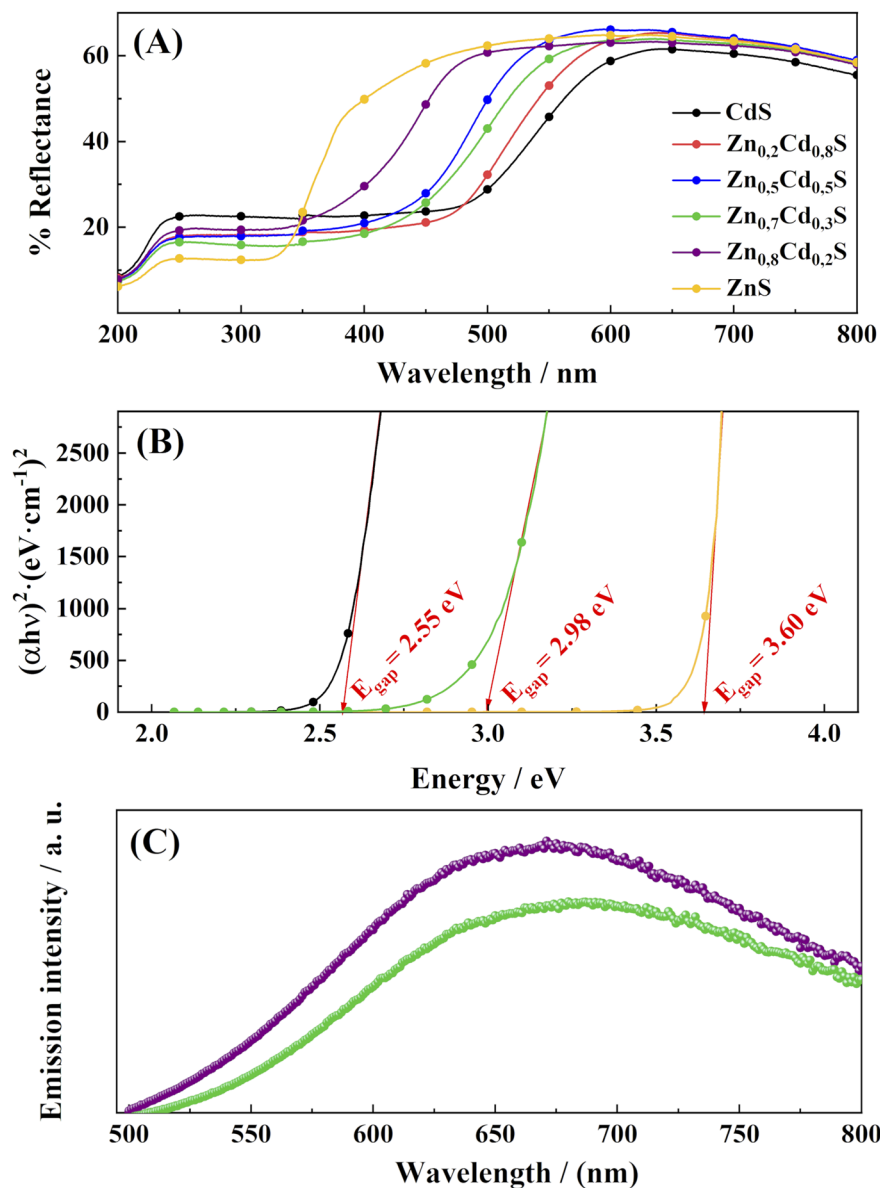**Fig. 3** (A) Diffuse reflectance spectra of the $Zn_{1-x}Cd_xS$ solid-state photocatalysts, with $x = 0$ to 1. (B) Tauc plot for determining the bandgap for $Zn_{0.7}Cd_{0.3}S$, CdS and ZnS. (C) Photoluminescence spectra for $Zn_{0.7}Cd_{0.3}S$ (green dots) and $Zn_{0.8}Cd_{0.2}S$ (purple dots) samples obtained under excitation at 440 nm, corresponding to the mean bandgap separation energy of both samples.

2.4 eV value reported by Ullah *et al.*[68] for CdS, and 3.6 eV reported by D'Amico *et al.*[69] for ZnS. In addition, a value of 2.98 eV was determined for the band gap of $Zn_{0.7}Cd_{0.3}S$ (*i.e.*, the material presenting the highest H_2 rate photochemical production in the next section). It can be clearly observed that the bandgap increases with the increasing content of Zn in the solid solution. Thus, the target material possesses a band gap value located between that of the pure CdS and pure ZnS (2.98 eV). Although the band gap energy is a fundamental parameter that can be modulated to achieve good photocatalytic activity,[32,33] the absolute position of the latter is not the only descriptor to be considered in semiconductor chemistry. Thus, to achieve a clear picture about the semiconductor behaviour, further descriptors must be studied, such as the electron–hole recombination

rate[70,71] or the position of both the VB and the CB. The latter was achieved by an electrochemical impedance study of the materials.

Fig. 3c shows the photoluminescence (PL) spectra of the spherical nanocrystals obtained in this work. The curve displays a broad emission, which shifts to a longer wavelength with higher cadmium content. The broad peak centered at ~640 nm and ~700 nm for $Zn_{0.8}Cd_{0.2}S$ and $Zn_{0.7}Cd_{0.3}S$, respectively, come from a trapped emission ascribed to the sulfur- and zinc-related vacancies and surface states.[72] The decrease in the photoluminescence intensity is due to the decrease in the number of point defects and suppressed recombination of photogenerated electron–hole pairs.[73] As was stablished in the literature, the electron recombination is directly related to the

PL intensity, as lower intensity indicates a reduced recombination rate and longer carrier lifetime.[74] These results explain the significant hydrogen production rate shown by the $Zn_{0.7}Cd_{0.3}S$ catalyst.

3.3 Mott–Schottky analysis

As the photocatalysts studied in this work are n-type semiconductors, the position of the valence flat band potential (V_{FB}) is estimated to be close to the conduction band. Thus, to estimate the former, several EIS experiments have been carried out in 0.1 M Na_2SO_3 and the Mott–Schottky analysis was performed (Fig. 4). The Mott–Schottky technique scans the electrochemical impedance response of the material in the region where no complete (electro)chemical reactions take place. Thus, the addition of the sacrificial agent is not needed to carry this measurement, as no hydrogen is photochemically generated during the measurement. Since the calculation of the flat-band potential allows the position of the conduction band to be estimated, the position of the valence band has been solved by applying the direct subtraction of the band gap calculated in the previous section from the V_{FB}. An energy diagram of the semiconductors is depicted in Fig. 5. Indeed, the position of the bands with respect to the redox couples for water splitting proves that the whole process is expected to take place while using these materials as photocatalytic suspensions in a photoreactor for water splitting. The value obtained for the conduction band of CdS was determined to be 6.2 eV, which is in agreement with that estimated by Kindig and Spicer (6.4 eV).[75] Similarly, the value of the conduction band for ZnS synthesized in this work is similar to that calculated by Yuhong Huang *et al.* (−8.62 eV to −6.04 eV).[76] On the other hand, the values for the CB obtained for the $Zn_{0.7}Cd_{0.3}S$ (−3.5 eV) in our work is higher than those obtained by other authors[77] for polycrystalline samples of similar composition (−4.3 eV). This change may have mainly resulted from the sample prepared by Arriaga *et al.*[77] being a mixture of wurtzite and sphalerite phases.
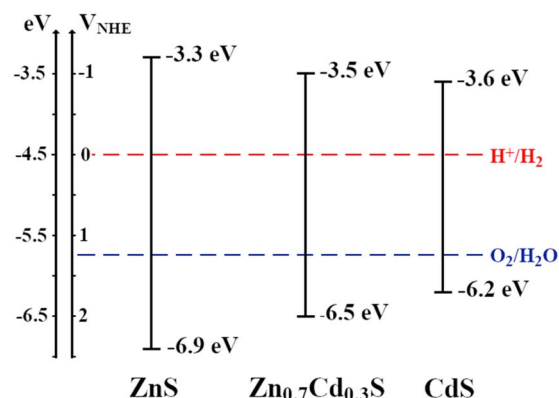

Fig. 5 Energy diagram of the valence and conduction bands of the synthesized semiconductors. The position of the conduction band has been estimated from Mott−Schottky analysis, and the value of the band gap was obtained from the diffuse reflectance spectra.

It is important to note that the catalysts must meet three different requirements for hydrogen production: (i) maintain adequate band edge energy for the overall water splitting; (ii) present band gap energy values lower than 3 eV;[33] and (iii) show high stability towards the photocatalytic reaction. Moreover, for those catalysts, it is also desirable to maintain the edge of the CB as close as possible to 3 eV *vs.* NHE (−7.5 eV).[77] By taking this into consideration, the CB of the ZnS is closer to 3 eV *vs.* NHE than the rest of the materials, however its band gap is too large to carry the photo water splitting (3.60 eV). CdS presents a good value for the band gap (2.55 eV), but the conduction band is too far from 3 eV *vs.* NHE. Thus, the $Zn_{0.7}Cd_{0.3}S$ is in a situation where all the requirements are fulfilled, with a band gap slightly lower than 3 eV (2.98 eV) and a conduction band that is closer to 3 eV *vs.* NHE than that of the CdS. These features, along with the role of the sacrificial agent and the decrease of electron–hole recombination enhanced by the small particle size,[78] boost the photocatalytic activity of $Zn_{0.7}Cd_{0.3}S$ towards water splitting.
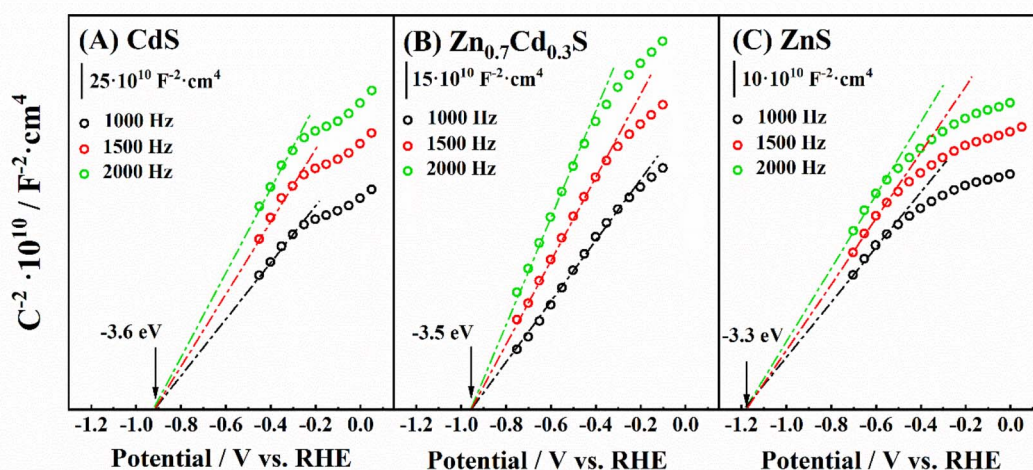

Fig. 4 Mott−Schottky obtained by measuring the capacitance at 1000, 1500 and 2000 Hz in a 0.1 M Na_2SO_3 solution by EIS for (A) ZnS, (B) CdS and (C) $Zn_{0.7}Cd_{0.3}S$.

3.4 Hydrogen production

Hydrogen production tests were performed using the home-made system[42] described in Section 2.4. To the best of our knowledge, this configuration has not been previously reported in the photochemistry field. Thus, it is important to mention its advantages, especially for the study of water splitting. Most of the research studies devoted to the photochemical production of hydrogen by water splitting use gas chromatography to characterize the catalytic activity of the materials. Thus, the experiments are carried in batch regime. This means that gas chromatography allows the detection of the accumulated hydrogen production at several times. Thus, after several batches, one can divide the generated hydrogen (normally expressed in mmol g_{cat}^{-1}) by the time (normally expressed in h) to achieve a value of the average rate production units in mmol g_{cat}^{-1} h^{-1}. However, the configuration presented in this work allows us to do the opposite. Here, the H_2 production rate is measured at every moment, and the integration of the area under de curve allows to solve the amount of total hydrogen generated during the process. This concept may be interesting as a starting point to study under *in situ* conditions how the hydrogen production rate is affected by different parameters (*i.e.*, changes in the wavelength of the irradiation light or in its intensity, addition of different concentrations of the sacrificial agent, *etc.*).

As a proof-of-principle of both the materials synthesized and the MS-coupled photochemical reactor developed in this work, the hydrogen photo-production rate was determined for pure CdS with sphalerite and wurtzite structural types (Fig. 6). Firstly, a fast response of the system towards a change in the wavelength was demonstrated. In this case, after 100 minutes of measuring under visible conditions, the light source was changed to UV, and thus an increase in the H_2 production rate was immediately detected (*i.e.*, a very fast response time of the MS configuration). This corroborates the capacity of the system to record changes in the production rate under *in situ* conditions. Moreover, this experiment also proves that the sphalerite structure presents slightly better photoactivity than the wurtzite one for hydrogen production under both visible and UV radiation. An analogous plot can be seen in Fig. 7 for $Zn_{1-x}Cd_xS$
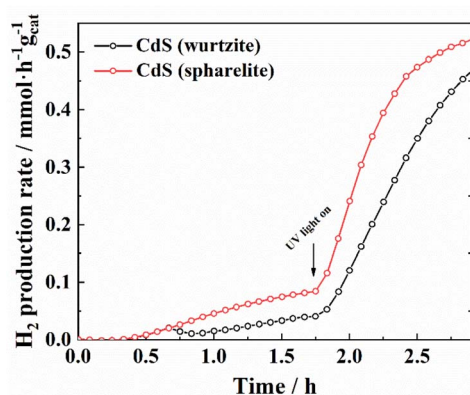
semiconductors synthesized in this work with sphalerite structure. Hydrogen production measurements were performed and monitored until the concentration of hydrogen production remained stable (100 min) under visible light irradiation. The light source was then changed to an ultraviolet lamp, and the samples were irradiated for another 100 minutes (the results have been separated into two different plots to better understand the integration of the signal and its mathematical limits).

As the values are easier to compare with the existing literature on H_2 production with sulfides, the accumulative hydrogen after *ca.* 2 h of production was resolved by integration of Fig. 7A for all the materials studied in this work. The values obtained for the visible light show that all the materials present the same production rate during the first 15 min upon illumination with visible light. However, from this point, the H_2 production rate varies for every material. Indeed, it is clear that both small or large amounts of Zn at the solid solution maintain photocatalytic behavior that is similar to those of the pure ZnS/CdS phases. Nevertheless, those materials with Zn content between $0.5 < x < 0.8$, particularly the $Zn_{0.7}Cd_{0.3}S$, have shown the fastest response towards photochemical H_2 generation. Fig. S2, ESI,† shows the H_2 production with and without a sacrificial agent for $Zn_{0.7}Cd_{0.3}S$ and $Zn_{0.8}Cd_{0.2}S$ and for the sacrificial agent alone, confirming that the high values of H_2 production are mainly due to our catalysts. As the results obtained by this method should be comparable with the existing literature, the data depicted in Fig. 7A have been integrated to achieve the amount of hydrogen generated during the 100 minutes of illumination with visible light (the total amount of

Fig. 6 Comparison of the hydrogen production rate for CdS with wurtzite and sphalerite structures.
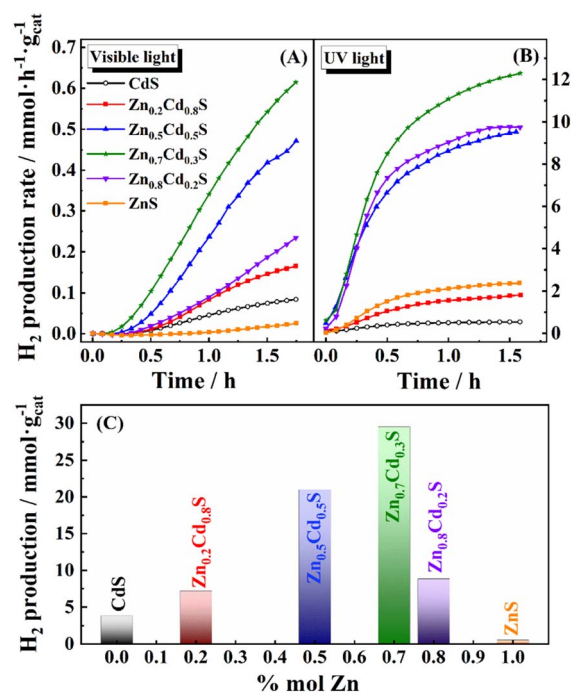

Fig. 7 Hydrogen production rate *vs.* time for the $Zn_{1-x}Cd_xS$ catalysts with different zinc contents using (A) visible and (B) UV light. (C) Maximum hydrogen production rate of $Zn_{1-x}Cd_xS$ *vs.* zinc content, using UV radiation.

Table 1 Hydrogen production for various catalysts based on the $Zn_{1-x}Cd_xS$ composition without cocatalyst. Sacrificial agents and their concentration used are also included

Catalyst	Cocatalyst	H_2 production (mmol g_{cat}^{-1})	Sacrificial agent	Year/reference
$Zn_{0.56}Cd_{0.44}S$	—	0.6	0.35 M Na_2SO_3 + 0.25 M Na_2S	2010 (ref. 53)
$Zn_{0.7}Cd_{0.3}S$	—	1.7	0.30 M Na_2SO_3 + 0.25 M Na_2S	2017 (ref. 79)
$Zn_{0.5}Cd_{0.5}S$	$Fe_{0.3}Pt_{0.7}$	4.5	0.35 M Na_2SO_3 + 0.25 M Na_2S	2017 (ref. 80)
$Zn_{0.7}Cd_{0.3}S$	—	29.5	0.35 M Na_2SO_3 + 0.25 M Na_2S	This work

H_2 over a specific period is the most common descriptor of a photochemical catalyst in literature). The results are presented in Fig. 7C. Hydrogen production obtained with $Zn_{0.7}Cd_{0.3}S$ attained a value of 29.5 mmol of H_2 per g_{cat} under visible radiation, which is higher than those reported by other authors studying zinc/cadmium sulphide-based composites. To prove this, some literature results are summarized in Table 1. In particular, Shu et al.[80] achieved lower production than those reported in the present work (4.5 mmol of H_2 per g_{cat}), but also used zinc/cadmium sulphide-based composites with sphalerite structures. On the other hand, a short survey of the production rates of similar catalyst compositions synthesized through different methods shows relatively low H_2 production compare with our material, with values between 0.6 and 1.7 mmol g_{cat}^{-1} (ref. 81) under visible light. It should be noted that the catalysts synthesized in this work have not been optimized. Furthermore, both noble metal and other co-catalysts have not been used yet, so further improvement in the activity is expected in future research for our materials.

4. Conclusions

In this work, a reactor has been coupled to a mass spectrometer detector as a method to measure the rate of a photochemical reaction under in situ conditions. The configuration allows us to directly measure the impact of experimental changes (e.g., energy of the irradiated light) during the photochemical process. This configuration allowed for the photochemical characterization of the H_2 production with Zn/Cd sulphide catalysts as a proof of concept. The physicochemical characterization of the catalysts indicates the formation of nanometric size powders, where the addition of Cd to the cubic structure of ZnS produces: (i) a significant reduction of the bandgap energy and (ii) an increase of the valence band energy. These two features, along with the lower recombination rate proved by photoluminescence measurements, propose that the $Zn_{0.7}Cd_{0.3}S$ material is the one with higher activity towards the photochemical water splitting. This was corroborated in the MS-coupled photochemical reactor, which showed a total production yield of 29.5 $mmol_{H_2} g_{cat}^{-1}$ over 100 min, along with a maximum production rate of 0.6 mmol $g_{cat}^{-1} h^{-1}$. Altogether, the setup presented in this work has been successfully proved as an innovative technique to achieve in situ information of the photocatalytic system.

Data availability

Data will be made available from the corresponding author upon request.

Author contributions

Modesto González-Rodríguez: writing – original draft, methodology; Sergio Díaz-Coello: writing – original draft, methodology; Selene Díaz-González: methodology; Michail Žitňan: methodology, Gustavo Galleani: methodology; Jose Joaquín Velázquez: methodology, Vicente Daniel Rodríguez: supervision; Elena Pastor: writing – review & editing, Pedro Núñez: conceptualization, supervision, writing – review & editing, funding acquisition.

Conflicts of interest

The authors declare that they have no known competing financial interests or personal relationships that could have appeared to influence the work reported in this paper.

Acknowledgements

References

1 S. Z. Baykara, Hydrogen as fuel: A critical technology?, Int. J. Hydrogen Energy, 2005, **30**(5), 545–553, DOI: **10.1016/j.ijhydene.2004.06.010**.

2 S. Verhelst, Recent progress in the use of hydrogen as a fuel for internal combustion engines, Int. J. Hydrogen Energy, 2014, **39**(2), 1071–1085, DOI: **10.1016/j.ijhydene.2013.10.102**.

3 T. Terlouw, C. Bauer, R. McKenna and M. Mazzotti, Large-scale hydrogen production via water electrolysis: a techno-economic and environmental assessment, Energy Environ. Sci., 2022, **15**(9), 3583–3602, DOI: **10.1039/d2ee01023b**.

4 Z. Yan, K. Yin, M. Xu, et al., Photocatalysis for synergistic water remediation and H2 production: A review, Chem. Eng. J., 2023, **472**, 145066, DOI: **10.1016/j.cej.2023.145066**.

© 2024 The Author(s). Published by the Royal Society of Chemistry

5 S. Chen, T. Takata and K. Domen, Particulate photocatalysts for overall water splitting, *Nat. Rev. Mater.*, 2017, **2**, 17050, DOI: **10.1038/natrevmats.2017.50**.

6 Q. Wang, T. Hisatomi, Q. Jia, *et al.*, Scalable water splitting on particulate photocatalyst sheets with a solar-to-hydrogen energy conversion efficiency exceeding 1%, *Nat. Mater.*, 2016, **15**(6), 611, DOI: **10.1038/nmat4589**.

7 A. Fujishima and K. Honda, Electrochemical Photolysis of Water at a Semiconductor Electrode, *Nature*, 1972, **238**, 37, DOI: **10.1038/238037a0**.

8 A. Fujishima, T. N. Rao and D. A. Tryk, Titanium Dioxide Photocatalysis, *J. Photochem. Photobiol., C*, 2000, **1**, 1.

9 A. J. Bard, Photoelectrochemistry and heterogeneous photo-catalysis at semiconductors, *J. Photochem.*, 1979, **10**(1), 59, DOI: **10.1016/0047-2670(79)80037-4**.

10 J. Prakash, P. Kumar, N. Saxena, *et al.*, CdS based 3D nano/micro-architectures: formation mechanism, tailoring of visible light activities and emerging applications in photocatalytic H_2 production, CO_2 reduction and organic pollutant degradation, *J. Mater. Chem. A*, 2023, **11**, 10015, DOI: **10.1039/d3ta00396e**.

11 H. Dong, G. Zeng, L. Tang, *et al.*, An overview on limitations of TiO_2-based particles for photocatalytic degradation of organic pollutants and the corresponding countermeasures, *Water Res.*, 2015, **79**, 128, DOI: **10.1016/j.watres.2015.04.038**.

12 Y. Ham, T. Hisatomi, Y. Goto, *et al.*, Flux-mediated doping of $SrTiO_3$ photocatalysts for efficient overall water splitting, *J. Mater. Chem. A*, 2016, **4**, 3027, DOI: **10.1039/c5ta04843e**.

13 R. Konta, T. Ishii, H. Kato and A. Kudo, Photocatalytic activities of noble metal ion doped $SrTiO_3$ under visible light irradiation, *J. Phys. Chem. B*, 2004, **108**, 8992, DOI: **10.1021/jp049556p**.

14 L. Díaz, V. D. Rodríguez, M. González-Rodríguez, *et al.*, M/TiO_2(M = Fe, Co, Ni, Cu, Zn) catalysts for photocatalytic hydrogen production under UV and visible light irradiation, *Inorg. Chem. Front.*, 2021, **8**, 3491, DOI: **10.1039/d0qi01311k**.

15 K. Maeda, D. Lu and K. Domen, Direct water splitting into hydrogen and oxygen under visible light by using modified TaON photocatalysts with d0 electronic configuration, *Chem.–Eur. J.*, 2013, **19**, 4986, DOI: **10.1002/chem.201300158**.

16 K. Maeda, T. Takata, M. Hara, *et al.*, GaN:ZnO solid solution as a photocatalyst for visible-light-driven overall water splitting, *J. Am. Chem. Soc.*, 2005, **127**, 8286, DOI: **10.1021/ja0518777**.

17 J. A. Nasir, Z. U. Rehman, S. N. A. Shah, A. Khan, I. S. Butler and C. R. A. Catlow, Recent developments and perspectives in CdS-based photocatalysts for water splitting, *J. Mater. Chem. A*, 2020, **8**, 20752–20780, DOI: **10.1039/d0ta05834c**.

18 G. Zuo, Y. Wang, W. L. Teo, *et al.*, Ultrathin $ZnIn_2S_4$ Nanosheets Anchored on Ti_3C_2TX MXene for Photocatalytic H_2 Evolution, *Angew. Chem., Int. Ed.*, 2020, **59**, 11287, DOI: **10.1002/anie.202002136**.

19 X. Chen, S. Shen, L. Guo and S. S. Mao, Semiconductor-based photocatalytic hydrogen generation, *Chem. Rev.*, 2010, **110**, 6503, DOI: **10.1021/cr1001645**.

20 A. Kudo and Y. Miseki, Heterogeneous photocatalyst materials for water splitting, *Chem. Soc. Rev.*, 2009, **38**, 253, DOI: **10.1039/b800489g**.

21 H. Du, K. Liang, C. Z. Yuan, *et al.*, Bare Cd1-xZnxS ZB/WZ Heterophase Nanojunctions for Visible Light Photocatalytic Hydrogen Production with High Efficiency, *ACS Appl. Mater. Interfaces*, 2016, **8**, 24550, DOI: **10.1021/acsami.6b06182**.

22 M. Liu, D. Jing, Z. Zhou and L. Guo, Twin-induced one-dimensional homojunctions yield high quantum efficiency for solar hydrogen generation, *Nat. Commun.*, 2013, **4**, 2278, DOI: **10.1038/ncomms3278**.

23 M. Huang, Z. Kong, Z. Ai, *et al.*, Twin $Zn_{1−x}Cd_xS$ Solid Solution: Highly Efficient Photocatalyst for Water Splitting, *Nano–Micro Small*, 2023, **20**, 2304784, DOI: **10.1002/smll.202304784**.

24 W. Zhang, Z. Zhong, Y. Wang and R. Xu, Doped solid solution: $(Zn_{0.95}Cu_{0.05})_{1-x}Cd_xS$ nanocrystals with high activity for H_2 evolution from aqueous solutions under visible light, *J. Phys. Chem. C*, 2008, **112**, 17635, DOI: **10.1021/jp8059008**.

25 L. Shang, B. Tong, H. Yu, *et al.*, CdS Nanoparticle-Decorated Cd Nanosheets for Efficient Visible Light-Driven Photocatalytic Hydrogen Evolution, *Adv. Energy Mater.*, 2016, **6**, 1501241, DOI: **10.1002/aenm.201501241**.

26 J. A. Villoria, R. M. Navarro-Yerga, S. M. Al-Zahrani and J. L. G. Fierro, Photocatalytic hydrogen production on $Cd_{1-x}Zn_xS$ solid solutions under visible light: Influence of thermal treatment, *Ind. Eng. Chem. Res.*, 2010, **49**, 6854, DOI: **10.1021/ie901718r**.

27 F. del Valle, A. Ishikawa, K. Domen, *et al.*, Influence of Zn concentration in the activity of $Cd_{1-x}Zn_xS$ solid solutions for water splitting under visible light, *Catal. Today*, 2009, **143**, 51, DOI: **10.1016/j.cattod.2008.09.024**.

28 M. Liu, L. Wang, G. Lu, X. Yao and L. Guo, Twins in $Cd_{1-x}Zn_xS$ solid solution: Highly efficient photocatalyst for hydrogen generation from water, *Energy Environ. Sci.*, 2011, **4**, 1372, DOI: **10.1039/c0ee00604a**.

29 C. Xing, Y. Zhang, W. Yan and L. Guo, Band structure-controlled solid solution of $Cd_{1-x}Zn_xS$ photocatalyst for hydrogen production by water splitting, *Int. J. Hydrogen Energy*, 2006, **31**, 2018, DOI: **10.1016/j.ijhydene.2006.02.003**.

30 F. Kurnia, J. A. Scott, H. Valanoor and J. N. Hart, A review of non-oxide semiconductors for photoelectrochemical water splitting, *J. Mater. Chem. C*, 2022, **11**, 802–826, DOI: **10.1039/d2tc02533g**.

31 M. M. Hoque, M. A. Zubair and R. N. Sajjad, Formation of wide-bandgap, highly transparent and compact $Cd_{1−x}Zn_xS$ films with dynamically controlled pH in chemical bath deposition, *J. Mater. Chem. C*, 2023, **13**, 6360, DOI: **10.1039/d3tc00450c**.

32 Z. Mei, M. Zhang, J. Schneider, *et al.*, Hexagonal $Zn_{1-x}Cd_xS$ ($0.2 \leq x \leq 1$) solid solution photocatalysts for H_2

generation from water, *Catal. Sci. Technol.*, 2017, **7**, 982, DOI: **10.1039/c6cy02572b**.

33 M. Huang, X. Luo, Z. Ai, *et al.*, Band Structure–Controlled $Zn_{1-x}Cd_xS$ Solid Solution for Photocatalytic Hydrogen Production Improvement *via* Appropriately Enhancing Oxidation Capacity, *Sol. RRL*, 2021, **5**, 2000685, DOI: **10.1002/solr.202000685**.

34 M. Matsumura, S. Furukawa, Y. Saho and H. Tsubomura, Cadmium sulfide photocatalyzed hydrogen production from aqueous solutions of sulfite: effect of crystal structure and preparation method of the catalyst, *J. Phys. Chem.*, 1985, **89**, 1327, DOI: **10.1021/j100254a001**.

35 M. K. Arora, A. S. K. Sinha and S. N. Upadhyay, Active Cadmium Sulfide Photocatalysts for Hydrogen Production from Water, *Ind. Eng. Chem. Res.*, 1998, **37**, 3950, DOI: **10.1021/ie970617y**.

36 C. Xing, Y. Zhang, W. Yan and L. Guo, Band structure-controlled solid solution of $Cd_{1-x}Zn_xS$ photocatalyst for hydrogen production by water splitting, *Int. J. Hydrogen Energy*, 2006, **31**, 2018, DOI: **10.1016/j.ijhydene.2006.02.003**.

37 M. Liu, L. Wang, G. Lu, X. Yao and L. Guo, Twins in $Cd_{1-x}Zn_xS$ solid solution: Highly efficient photocatalyst for hydrogen generation from water, *Energy Environ. Sci.*, 2011, **4**, 1372, DOI: **10.1039/c0ee00604a**.

38 J. Chen, Z. Shen, S. Lv, *et al.*, Fabricating sandwich-shelled ZnCdS/ZnO/ZnCdS dodecahedral cages with "one stone" as Z-scheme photocatalysts for highly efficient hydrogen production, *J. Mater. Chem. A*, 2018, **6**, 19631, DOI: **10.1039/c8ta07362g**.

39 Y. Liu, X. Zheng, Y. Yang, *et al.*, Recent Advances in the Hydrogen Evolution Reaction of $Zn_xCd_{1-x}S$-Based Photocatalysts, *Sol. RRL*, 2022, **6**, 2101061, DOI: **10.1002/solr.202101061**.

40 Z. Zhou, F. Han, L. Guo and O. V. Prezhdo, Understanding divergent behaviors in the photocatalytic hydrogen evolution reaction on CdS and ZnS: A DFT based study, *Phys. Chem. Chem. Phys.*, 2016, **18**, 16862, DOI: **10.1039/c6cp02599d**.

41 H. Yan, J. Yang, G. Ma, *et al.*, Visible-light-driven hydrogen production with extremely high quantum efficiency on Pt-PdS/CdS photocatalyst, *J. Catal.*, 2009, **266**, 165, DOI: **10.1016/j.jcat.2009.06.024**.

42 J. J. Velázquez, R. Fernández-González, L. Díaz, E. Pulido-Melián, V. D. Rodríguez and P. Núñez, Effect of reaction temperature and sacrificial agent on the photocatalytic H_2-production of Pt-TiO_2, *J. Alloys Compd.*, 2017, **721**, 405, DOI: **10.1016/j.jallcom.2017.05.314**.

43 H. Zhao, J. Wang, Y. Dong and P. Jiang, Noble-Metal-Free Iron Phosphide Cocatalyst Loaded Graphitic Carbon Nitride as an Efficient and Robust Photocatalyst for Hydrogen Evolution under Visible Light Irradiation, *ACS Sustain. Chem. Eng.*, 2017, **5**, 8053, DOI: **10.1021/acssuschemeng.7b01665**.

44 H. Nishikiori, N. Harata, S. Yamaguchi, *et al.*, Formation of CuO on TiO_2 surface using its photocatalytic activity, *Catalysts*, 2019, **9**, 383, DOI: **10.3390/catal9040383**.

45 Y. Zhao, W. Xue, W. Sun, *et al.*, Highly efficient twinned $Mn_xCd_{1-x}S$ homojunction photocatalyst modified by noble metal-free $Ni_{12}P_5$ for H_2 evolution under visible light, *Int. J. Hydrogen Energy*, 2023, **48**, 31161, DOI: **10.1016/j.ijhydene.2023.04.215**.

46 A. T. Hoang, A. Pandey, W. H. Chen, *et al.*, Hydrogen Production by Water Splitting with Support of Metal and Carbon-Based Photocatalysts, *ACS Sustain. Chem. Eng.*, 2023, **11**, 1221, DOI: **10.1021/acssuschemeng.2c05226**.

47 Y. Xu, Y. Gong, H. Ren, *et al.*, Insight into enhanced photocatalytic H_2 production by $Ni(OH)_2$-decorated $Zn_xCd_{1-x}S$ nanocomposite photocatalysts, *J. Alloys Compd.*, 2018, **735**, 2551, DOI: **10.1016/j.jallcom.2017.11.388**.

48 T. Bai, X. Shi, M. Liu, *et al.*, A metal-organic framework-derived $Zn_{1-x}Cd_xS$/CdS heterojunction for efficient visible light-driven photocatalytic hydrogen production, *Dalton Trans.*, 2021, **50**, 6064, DOI: **10.1039/d1dt00667c**.

49 M. Chen, X. Huang, C. Chen, W. Hou and Y. Xu, M-Dependent activity of MCo_2O_4 spinels for water splitting and H_2 production on $Zn_{0.5}Cd_{0.5}S$ under visible light, *Appl. Catal., B*, 2021, **298**, 120469, DOI: **10.1016/j.apcatb.2021.120469**.

50 J. Dong, W. Fang, W. Xia, Q. Lu and X. Zeng, Facile preparation of $Zn_xCd_{1-x}S$/ZnS heterostructures with enhanced photocatalytic hydrogen evolution under visible light, *RSC Adv.*, 2021, **11**, 21642, DOI: **10.1039/d1ra03195c**.

51 Y. J. Yuan, D. Chen, Z. T. Yu and Z. G. Zou, Cadmium sulfide-based nanomaterials for photocatalytic hydrogen production, *J. Mater. Chem. A*, 2018, **6**, 11606, DOI: **10.1039/c8ta00671g**.

52 D. J. Fermín, E. A. Ponomarev and L. M. Peter, A Kinetic Study of CdS Photocorrosion by Intensity Modulated Photocurrent and Photoelectrochemical Impedance Spectroscopy, *J. Mater. Chem. A*, 1999, **473**, 192, DOI: **10.1016/S0022-0728(99)00109-6**.

53 L. Wang, W. Wang, M. Shang, W. Yin, S. Sun and L. Zhang, Enhanced photocatalytic hydrogen evolution under visible light over $Cd_{1-x}Zn_xS$ solid solution with cubic zinc blend phase, *Int. J. Hydrogen Energy*, 2010, **35**, 19, DOI: **10.1016/j.ijhydene.2009.10.084**.

54 N. Bao, L. Shen, T. Takata and K. Domen, Self-templated synthesis of nanoporous CdS nanostructures for highly efficient photocatalytic hydrogen production under visible light, *Chem. Mater.*, 2008, **20**, 110, DOI: **10.1021/cm7029344**.

55 W. Q. Peng, G. W. Cong, S. C. Qu and Z. G. Wang, Synthesis and photoluminescence of ZnS:Cu nanoparticles, *Opt. Mater.*, 2006, **29**, 313, DOI: **10.1016/j.optmat.2005.10.003**.

56 K. Sivula, Mott-Schottky analysis of photoelectrodes: Sanity checks are needed, *ACS Energy Lett.*, 2021, **6**, 2549, DOI: **10.1021/acsenergylett.1c01245**.

57 S. Oros-Ruiz, A. Hernández-Gordillo, C. García-Mendoza, A. A. Rodríguez-Rodríguez and R. Gómez, Comparative activity of CdS nanofibers superficially modified by Au, Cu, and Ni nanoparticles as co-catalysts for photocatalytic hydrogen production under visible light, *J. Chem. Technol. Biotechnol.*, 2016, **91**, 2205, DOI: **10.1002/jctb.4992**.

58 F. A. Mir, I. Chattarjee, A. A. Dar, K. Asokan and G. M. Bhat, Preparation and characterizations of cadmium sulfide nanoparticles, *Optik*, 2015, **126**, 1240, DOI: 10.1016/j.ijleo.2015.03.022.

59 D. Rodic, V. Spasojevic and A. Bajorek, Similarity of Structure Properties of $Hg_{1-x}Mn_xS$ and $Cd_{1-x}Mn_xS$ (Structure Properties of HgMnS and CdMnS), *J. Magn. Magn. Mater.*, 1996, **152**, 159, DOI: 10.1016/0304-8853(95)00435-1.

60 H. Sowa, On the mechanism of the pressure-induced wurtzite- to NaCl-type phase transition in CdS: An X-ray diffraction study, *Solid State Sci.*, 2005, **7**, 73, DOI: 10.1016/j.solidstatesciences.2004.10.011.

61 R. D. Shannon, Revised Effective Ionic Radii and Systematic Studies of Interatomic Distances in Halides and Chalcogenides, *Acta Crystallogr.*, 1976, **A32**, 751, DOI: 10.1107/S0567739476001551.

62 R. D. Shannon and C. T. Prewitt, Effective ionic radii in oxides and fluorides, *Acta Crystallogr.*, 1969, **B25**, 925, DOI: 10.1107/S0567740869003220.

63 S. D. Scott and H. L. Barnes, Sphalerite-wurtzite equilibria and stoichiometry, *Geochim. Cosmochim. Acta*, 1972, **36**, 1275, DOI: 10.1016/0016-7037(72)90049-X.

64 X. M. Meng, J. Liu, Y. Jiang, *et al.*, Structure- and size-controlled ultrafine ZnS nanowires, *Chem. Phys. Lett.*, 2003, **382**, 434, DOI: 10.1016/j.cplett.2003.10.093.

65 J. Tauc, R. Grigorovici and A. Vancu, Optical Properties and Electronic Structure of Amorphous Germanium, *Phys. Status Solidi B*, 1966, **15**, 627, DOI: 10.1002/pssb.19660150224.

66 P. Kubelka and F. Munk, An Article on Optics of Paint Layers, *Fuer Tekn. Physik.*, 1931, **12**, 593–593.

67 D. Li, Y. Liu, M. de la Mata, *et al*, Strain-induced spatially indirect exciton recombination in zinc-blende/wurtzite CdS heterostructures, *Nano Res.*, 2015, **8**, 3035, DOI: 10.1007/s12274-015-0809-8.

68 S. Ullah, A. Bouich, H. Ullah, B. Mari and M. Mollar, Comparative study of binary cadmium sulfide (CdS) and tin disulfide (SnS_2) thin buffer layers, *Sol. Energy*, 2020, **208**, 637, DOI: 10.1016/j.solener.2020.08.036.

69 P. D'Amico, A. Calzolari, A. Ruini and A. Catellani, New energy with ZnS: Novel applications for a standard transparent compound, *Sci. Rep.*, 2017, **7**, 16805, DOI: 10.1038/s41598-017-17156-w.

70 R. Marschall, Semiconductor composites: Strategies for enhancing charge carrier separation to improve photocatalytic activity, *Adv. Funct. Mater.*, 2014, **24**, 2421, DOI: 10.1002/adfm.201303214.

71 L. Cheng, Q. Xiang, Y. Liao and H. Zhang, CdS-Based photocatalysts, *Energy Environ. Sci.*, 2018, **11**, 1362, DOI: 10.1039/c7ee03640j.

72 V. G. Klyuev, D. V. Volykhin, O. V. Ovchinnikov and I. Sergey, Pokutnyi Relationship between structural and optical properties of colloidal $Cd_xZn_{1-x}S$ quantum dots in gelatin, *J. Nanophotonics*, 2016, **10**(3), 033507, DOI: 10.1117/1.JNP.10.033507.

73 J. Dong, W. Fang, W. Xia, Q. Lu and X. Zeng, Facile preparation of $Zn_xCd_{1-x}S$/ZnS heterostructures with enhanced photocatalytic hydrogen evolution under visible light, *RSC Adv.*, 2021, **11**(35), 21642–21650, DOI: 10.1039/d1ra03195c.

74 Y. Shang, C. Wang, C. Yan, F. Jing, M. Roostaeinia, Y. Wang, G. Chen and C. Lv, An Efficient and Multifunctional S-Scheme Heterojunction Photocatalyst Constructed by Tungsten Oxide and Graphitic Carbon Nitride: Design and Mechanism Study, *J. Colloid Interface Sci.*, 2023, **634**, 195–208, DOI: 10.1016/J.JCIS.2022.12.039.

75 N. B. Kindig and W. E. Spicer, Band Structure of Cadmium Sulfide – Photoemission Studies, *Phys. Rev.*, 1964, **138**, 561, DOI: 10.1103/PhysRev.138.A561.

76 Y. Huang, Z. Zhang, F. Ma, P. K. Chu, C. Dong and X. Wei, First-principles calculation of the band structure, electron states, and optical properties of Cr-doped ZnS double-wall nanotubes, *Comput. Mater. Sci.*, 2015, **101**, 1, DOI: 10.1016/j.commatsci.2015.01.011.

77 L. G. Arriaga and A. M. Fernández, Determination of flat band potential and photocurrent response in (Cd,Zn)S used in photoelectrolysis process, *Int. J. Hydrogen Energy*, 2002, **27**, 27, DOI: 10.1016/S0360-3199(01)00084-2.

78 K. Maeda, Photocatalytic water splitting using semiconductor particles: History and recent developments, *J. Photochem. Photobiol., C*, 2011, **12**, 237, DOI: 10.1016/j.jphotochemrev.2011.07.001.

79 M. Kaur and C. M. Nagaraja, Template-Free Synthesis of $Zn_{1-x}Cd_xS$ Nanocrystals with Tunable Band Structure for Efficient Water Splitting and Reduction of Nitroaromatics in Water, *ACS Sustain. Chem. Eng.*, 2017, **5**, 4293, DOI: 10.1021/acssuschemeng.7b0032581.

80 D. Shu, H. Wang, Y. Wang, *et al.*, Composition dependent activity of $Fe_{1-x}Pt_x$ decorated ZnCdS nanocrystals for photocatalytic hydrogen evolution, *Int. J. Hydrogen Energy*, 2017, **42**, 20888, DOI: 10.1016/j.ijhydene.2016.12.037.

81 L. Wang, W. Wang, M. Shang, W. Yin, S. Sun and L. Zhang, Enhanced photocatalytic hydrogen evolution under visible light over $Cd_{1-x}Zn_xS$ solid solution with cubic zinc blend phase, *Int. J. Hydrogen Energy*, 2010, **35**, 19, DOI: 10.1016/j.ijhydene.2009.10.084.